THE JOURNAL OF PHYSICAL CHEMISTRY A

Article

Cite This: J. Phys. Chem. A 2019, 123, 8099−8108

pubs.acs.org/JPCA

Singlet−Triplet Inversion in Heptazine and in Polymeric Carbon Nitrides

Johannes Ehrmaier,[†] Emily J. Rabe,[‡] Sarah R. Pristash,[‡] Kathryn L. Corp,[‡] Cody W. Schlenker,[‡] Andrzej L. Sobolewski,[§] and Wolfgang Domcke*[,†]

[†]Department of Chemistry, Technical University of Munich, D-85747 Garching, Germany

[‡]Department of Chemistry, University of Washington, Seattle, Washington 98195, United States

[§]Institute of Physics, Polish Academy of Sciences, PL-02-668 Warsaw, Poland

Supporting Information

ABSTRACT: According to Hund's rule, the lowest triplet state (T_1) is lower in energy than the lowest excited singlet state (S_1) in closed-shell molecules. The exchange integral lowers the energy of the triplet state and raises the energy of the singlet state of the same orbital character, leading to a positive singlet−triplet energy gap (Δ_{ST}). Exceptions are known for biradicals and charge-transfer excited states of large molecules in which the highest occupied molecular orbital (HOMO) and the lowest unoccupied molecular orbital (LUMO) are spatially separated, resulting in a small exchange integral. In the present work, we discovered with ADC(2), CC2, EOM-CCSD, and CASPT2 calculations that heptazine (1,3,4,6,7,9,9b-heptaazaphenalene or tri-*s*-triazine) exhibits an inverted S_1/T_1 energy gap ($\Delta_{ST} \approx -0.25$ eV). This appears to be the first example of a stable closed-shell organic molecule exhibiting S_1/T_1 inversion at its equilibrium geometry. The origins of this phenomenon are the nearly pure HOMO−LUMO excitation character of the S_1 and T_1 states and the lack of spatial overlap of HOMO and LUMO due to a unique structure of these orbitals of heptazine. The S_1/T_1 inversion is found to be extremely robust, being affected neither by substitution of heptazine nor by oligomerization of heptazine units. Using time-resolved photoluminescence and transient absorption spectroscopy, we investigated the excited-state dynamics of 2,5,8-tris(4-methoxyphenyl)-1,3,4,6,7,9,9b-heptaazaphenalene (TAHz), a chemically stable heptazine derivative, in the presence of external heavy atom sources as well as triplet-quenching oxygen. These spectroscopic data are consistent with TAHz singlet excited state decay in the absence of a low-energy triplet loss channel. The absence of intersystem crossing and an exceptionally low radiative rate result in unusually long S_1 lifetimes (of the order of hundreds of nanoseconds in nonaqueous solvents). These features of the heptazine chromophore have profound implications for organic optoelectronics as well as for water-splitting photocatalysis with heptazine-based polymers (e.g., graphitic carbon nitride) which have yet to be systematically explored and exploited.

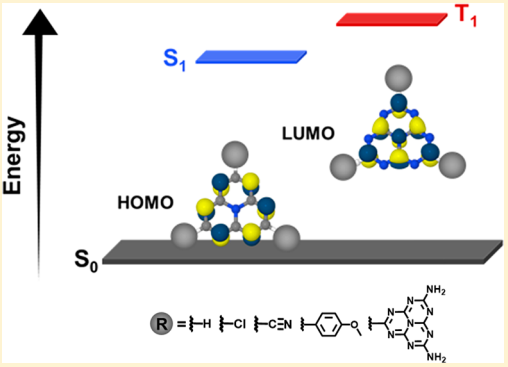

1. INTRODUCTION

It is textbook knowledge that the lowest triplet excited state (T_1) is located below the lowest singlet excited state (S_1) in closed-shell organic molecules, an example of Hund's multiplicity rule.[1] This rule is taken into account in the well-known Jablonski diagram which predicts that the S_1 state can be depopulated by spin−orbit-induced intersystem crossing (ISC) to the lower-lying triplet states. For excited states with the same orbital composition, the S_1/T_1 energy gap is determined by the exchange integral, which in general is large in organic chromophores at their ground-state equilibrium geometry and stabilizes the T_1 state relative to the S_1 state. In extended conjugated systems, the energy of the T_1 state can be lower than the energy of the S_1 state by an electron volt or more.[2]

According to current knowledge, there exist few, if any, stable aromatic molecules which violate Hund's multiplicity rule for their S_1 and T_1 states. Koseki et al. found a violation of Hund's multiplicity rule for the nonalternant hydrocarbons propalene, pentalene, and heptalene with Pariser−Parr−Pople (PPP) configuration interaction (CI) calculations when the structures were constrained to have high (D_{2h}) symmetry.[3] However, the S_1/T_1 inversion disappears at the relaxed (C_{2h}) symmetry of these systems.[3]

It has been noted that the exchange integral can become very small when the highest occupied molecular orbital (HOMO) and the lowest unoccupied molecular orbital (LUMO) are spatially nonoverlapping. In such cases, near degeneracy of the S_1 and T_1 states can be expected. This applies, in particular, for charge-transfer (CT) excited states in extended systems[4−7] and for biradicals.[8,9] Nearly degenerate S_1

Received: June 30, 2019
Revised: August 28, 2019
Published: August 29, 2019

DOI: 10.1021/acs.jpca.9b06215
J. Phys. Chem. A 2019, 123, 8099−8108

and T_1 states are favorable for organic optoelectronics, because so-called thermally activated delayed fluorescence may lead to a significant enhancement of the quantum efficiency of organic light-emitting diodes (OLEDs).[10,11] This discovery motivated the synthesis of a large variety of supramolecular systems with low-lying CT states with nonoverlapping HOMOs and LUMOs; see, for example, refs 12 and 13 for reviews.

In the present article, we report conclusive evidence of a significant and robust inversion of the energies of the S_1 and T_1 states for a comparatively simple and compact organic chromophore, the heptazine (1,3,4,6,7,9,9b-heptaazaphenalene or tri-*s*-triazine) molecule ($C_6N_7H_3$). In heptazine (Hz), the S_1/T_1 near degeneracy arises from the peculiar and rigid nuclear geometry as well as from a specific and unusual structure of the HOMO and the LUMO. The HOMO is exclusively located on the six peripheral nitrogen atoms of Hz, whereas the LUMO is exclusively located on the six carbon atoms and the central nitrogen atom. The HOMO−LUMO excitation therefore is an "internal" CT excitation in this chromophore, which results in a near-zero exchange integral. As discussed below, the stabilization of the S_1 state by spin polarization[3,14] leads to S_1/T_1 inversion.

The elimination of the ISC deactivation channel of the S_1 state of Hz by S_1/T_1 inversion has obvious implications for two large and active research areas: organic optoelectronics[10−13] and water-oxidation photocatalysis.[15−17] While Hz-derived materials were occasionally tested for OLEDs and received vast attention as photocatalysts for hydrogen evolution by water splitting, the potential of S_1/T_1 inversion in the Hz chromophore has not been recognized so far and therefore has not been systematically exploited in either research area.

2. METHODS

2.1. Electronic-Structure Calculations. The ground-state equilibrium geometries of Hz and several derivatives of Hz were optimized with the second-order Møller−Plesset (MP2) method. The structures are planar and exhibit D_{3h} symmetry.

The vertical excitation energies of the singlet and triplet excited states were computed with four wave-function-based electronic-structure methods and with time-dependent density functional theory (TDDFT). We employed a single-reference propagator method (second-order algebraic diagrammatic construction (ADC(2)),[18] two single-reference coupled-cluster methods (approximate second-order coupled cluster (CC2)[19] and equation-of-motion singles-and-doubles coupled cluster (EOM-CCSD)[20]), and a multiconfiguration self-consistent-field multireference perturbation method (CASSCF/CASPT2).[21,22] The active space for the CASSCF calculations for Hz consisted of 12 electrons in 12 orbitals, five occupied and five unoccupied π orbitals as well as the highest occupied n orbital and the lowest unoccupied σ orbital. Because the S_1 and T_1 states are nearly pure HOMO (π) to LUMO (π^*) excitations, their energies are not sensitive to the choice of the active space. The TDDFT calculations were performed with five widely used exchange−correlation functionals, the three-parameter Becke, Lee, Yang, Parr functional (B3LYP),[23,24] the Perdew−Burke−Ernzerhof functional (PBE0),[25] the Minnesota 06 functional (M06-2X),[26] and two range-separated functionals, CAM-B3LYP[27] and ωB97XD,[28] which are specifically designed to describe CT states.

The equilibrium geometries of the S_1 and T_1 excited states were optimized with the ADC(2) method, and adiabatic (minimum-to-minimum) excitation energies were calculated. To characterize the excited-state potential-energy (PE) surfaces in the vicinity of the Franck−Condon (FC) region, linearly interpolated scans in Cartesian coordinates between the S_0, S_1, and T_1 minima were computed.

Dunning's correlation-consistent double-ζ basis set (cc-pVDZ)[29] was used for all electronic-structure calculations. Calculations for Hz with the triple-ζ basis set (cc-pVTZ) and with the augmented double-ζ basis set (aug-cc-pVDZ) confirmed that the S_1 and T_1 excitation energies are insensitive to extensions of the double-ζ basis set. The MP2, ADC(2), and CC2 calculations were performed with the TURBOMOLE program package.[30] For the EOM-CCSD calculations the Q-Chem program[31] was used. The MOLPRO package[32] was used for the CASSCF/CASPT2 calculations. The DFT and TDDFT calculations were performed with either TURBOMOLE or Q-Chem.

2.2. Experimental Methods. The experimental investigations were performed for TAHz in toluene solution, because this compound is chemically easier to handle than heptazine itself, which rapidly hydrolyzes in the presence of visible light and traces of water.[33]

2.2.1. Sample Preparation. TAHz was synthesized and characterized as previously described.[34] To prepare samples for air-free and low-temperature emission measurements, we dispersed TAHz in polystyrene (PS) with and without a heavy atom source, diiodooctane (DIO), and drop-cast films in an argon glovebox, a method used previously in our group to measure triplet emission.[35] These films were then mounted in a Janis STVP-100 optical cryostat for low-temperature photoluminescence (PL) measurements. Air-free solution measurements were made and sealed inside an argon-filled glovebox or purged with argon.

2.2.2. Time-Correlated Single Photon Counting (TCSPC). TCSPC measurements were taken of TAHz solutions using a PicoQuant FluoTime 100 with 375 nm laser diode excitation. Emission was detected over a 4 μs time range and was triggered using an external function generator at 250 kHz. All solutions had a concentration of 33 μM in toluene, unless otherwise stated. Solutions without oxygen were purged with argon gas or made in an argon glovebox. Solutions with oxygen were either opened to air and air was bubbled in for 5 min, or they were prepared in ambient atmosphere. Samples with ethyl iodide (EtI) were made in a 50:50 mixture of toluene and EtI.

2.2.3. Time-Resolved Photoluminescence (TR-PL). TR-PL spectra were collected using a Hamamatsu streak camera (C10910) with a slow-sweep unit (M10913-01) in photon counting mode. Samples were irradiated with 50 fs pulses at 365 nm and 1 kHz pump from a Coherent/Light Conversion OPerA solo optical parametric amplifier (OPA). Pump fluence was 7.2×10^{11} photons cm^{-3}.

2.2.4. Transient Absorption. Samples were irradiated with the 365 nm (3×10^{14} photons/cm^3/pulse) output of a Coherent, Inc./Light Conversion OPerA Solo OPA that was pumped with 50 fs pulses from a 1 kHz Ti:sapphire amplifier (Libra-HE, Coherent, Inc.). White-light probe pulses (2 kHz) were generated and electronically delayed using the EOS transient absorption system (Ultrafast Systems Inc.). Spectra were collected with a CMOS sensor and InGaAs fiber-coupled multichannel photodiode array spectrometer and plotted as the differential optical density, $\Delta OD(\lambda,t) = Pump_{on}(\lambda,t) - Pump_{off}(\lambda)$. A reference line was monitored to account for fluctuations in the probe beam. Kinetics were recorded with random time steps to minimize any influence of sample

DOI: 10.1021/acs.jpca.9b06215
J. Phys. Chem. A 2019, 123, 8099−8108

degradation or variations in pump power during an experiment. Spectra were measured in a 2 mm path length quartz cuvette with continuous stirring. Surface Xplorer software (Ultrafast Systems) was used to collect spectra, and OriginPro 9.1.0 was used to process, analyze, and plot the data.

3. RESULTS

3.1. Heptazine. The vertical singlet and triplet excitation energies of the two lowest $\pi\pi^*$ and the two lowest $n\pi^*$ states of Hz calculated with the ADC(2) method are given in Table 1. In the singlet manifold, the Hz chromophore exhibits a low-lying (2.57 eV) $\pi\pi^*$ state of $^1A_2'$ symmetry (S_1), followed by two $n\pi^*$ states of $^1A_1''$ and $^1E''$ symmetry, respectively (S_2, S_3). The second $\pi\pi^*$ state of E′ symmetry (S_4) is located at 4.43 eV excitation energy at the ADC(2) level. While the S_1–S_0 transition is dipole-forbidden in D_{3h} symmetry, the second $\pi\pi^*$ state carries significant oscillator strength. In polymeric carbon nitride (melon), the S_1 state is weakly allowed due to vibronic intensity borrowing from higher allowed states as well as slight out-of-plane distortions of the Hz frame. The S_1 absorption can be seen as a faint tail extending to longer wavelengths (≈600 nm). The $S_4(\pi\pi^*)$ state gives rise to the pronounced absorption threshold of melon near 400 nm.[15]

Table 1. Vertical Excitation Energies (in eV) of the Lowest Four Singlet and Triplet Excited States of Hz, Calculated with the ADC(2) Method with the cc-pVDZ Basis Set[a]

symmetry	singlet	triplet
A_2'	2.569	2.851
A_1''	3.758	3.755
E″	3.845	3.819
E′	4.430	3.667

[a]The geometry was optimized at the MP2/cc-pVDZ level.

In the triplet manifold, the low-lying $^3A_2'$ state at 2.85 eV (T_1) is followed by the $^3E'$ state (T_2) at 3.67 eV, which is almost 0.8 eV lower in energy than the corresponding singlet state ($^1E'$ (S_4)). The next two states are the nondegenerate $^3A_1''$ state (T_3) and the degenerate $^3E''$ state (T_4); see Table 1. No experimental data on the excitation energies of the triplet states of Hz are available. Remarkably, the energy of the S_1 state is below the energy of the T_1 state in Hz. The S_1/T_1 vertical energy gap is defined as $\Delta_{ST} = E_{S_1} - E_{T_1}$. For Hz, $\Delta_{ST} = -0.28$ eV. For the two $n\pi^*$ states (S_2/T_3 and S_3/T_2), the energies of the singlet and triplet states of the same spatial symmetry are almost degenerate, with the singlet energies being slightly higher than the corresponding triplet energies; see Table 1.

The inverted ordering of the S_1 and T_1 states ($\Delta_{ST} < 0$) in Hz and in derivatives of Hz is the main focus of the present article. We therefore concentrate on the lowest singlet and triplet states in what follows. Both states are nearly pure HOMO–LUMO excitations (the weight of the HOMO–LUMO configuration is 96.4% for S_1, 98.4% for T_1 at the ADC(2) level). The highest occupied and the lowest unoccupied Hartree–Fock orbitals of Hz are displayed in Figure 1. It can be seen that the HOMO is exclusively localized on the peripheral nitrogen atoms, while the LUMO is exclusively localized on the carbon atoms and on the central nitrogen atom. As a result of this pattern, the spatial overlap of HOMO and LUMO is essentially zero. The HOMO–LUMO transition therefore can be considered as an intramolecular CT transition: one electronic charge is transferred from the peripheral nitrogen atoms to the carbon atoms and the central nitrogen atom. Due to D_{3h} symmetry, the electric dipole moments of the ground state and the nondegenerate excited states are zero. A similar effect of short-range charge transfer has also been reported for boron-centered azatriangulene molecules, which exhibit a small but positive singlet–triplet gap and are promising candidates for OLEDs.[36]

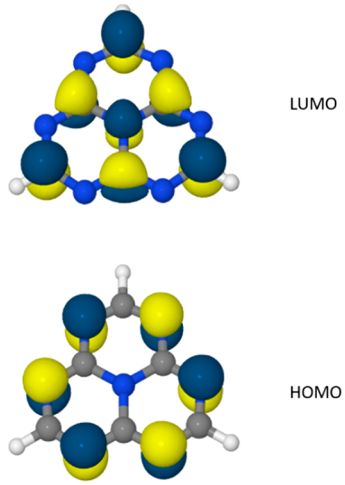

Figure 1. Highest occupied (HOMO) and lowest unoccupied (LUMO) Hartree–Fock molecular orbitals of Hz.

The lack of spatial overlap of HOMO and LUMO has two consequences: (i) the S_1–S_0 transition dipole moment is unusually small, and (ii) the exchange integral, which is primarily responsible for the singlet–triplet energy gap, is very small, resulting in a near degeneracy of S_1 and T_1 states. In this situation, spin polarization, which stabilizes the singlet state relative to the triplet state,[3,14] becomes relevant and leads to the inversion of the S_1 and T_1 states; see below.

To confirm the S_1/T_1 inversion in Hz predicted by ADC(2), we computed the vertical S_1 and T_1 excitation energies with the CC2, EOM-CCSD, and CASSCF/CASPT2 methods. The results are shown in Table 2. All four wave-function-based methods predict that the S_1 energy is 0.2–0.3 eV below the T_1 energy. The ADC(2), CC2, and EOM-CCSD vertical excitation energies agree within 0.2 eV, while the CASSCF/CASPT2 energies are 0.3–0.4 eV lower than the ADC(2)

Table 2. Vertical Excitation Energies (in eV) of the S_1 and T_1 Excited States of Hz and Singlet–Triplet Energy Gap Δ_{ST}, Calculated with Different Methods with the cc-pVDZ Basis Set[a]

method	S_1	T_1	Δ_{ST}
ADC(2)	2.569	2.851	−0.282
CC2	2.676	2.947	−0.271
EOM-CCSD	2.781	2.963	−0.182
CASPT2	2.326	2.551	−0.225
TDDFT/B3LYP	2.818	2.603	0.215
TDDFT/PBE0	2.924	2.682	0.242
TDDFT/M06-2X	3.048	2.835	0.213
TDDFT/CAM-B3LYP	3.060	2.817	0.243
TDDFT/wB97X-D	3.107	2.876	0.231

[a]The geometry was optimized at the MP2/cc-pVDZ level.

DOI: 10.1021/acs.jpca.9b06215
J. Phys. Chem. A 2019, 123, 8099–8108

energies. Because of the very low oscillator strength of the S_1-S_0 transition, no accurate experimental data are available for the vertical excitation energy of the S_1 state of Hz.

The close agreement of the four ab initio wave function methods based on different approximation schemes for electron correlation reveals that the S_1/T_1 inversion in Hz is not the result of intricate electron correlation effects. It results from the unusually small exchange integral (which can be guessed by inspection of the HOMO and the LUMO as discussed above) and spin polarization.[14] In the restricted orbital picture, spin polarization in the singlet state is reflected by a slightly higher weight of doubly excited configurations (and correspondingly a lower weight of the HOMO−LUMO configuration) in the singlet wave function than in the triplet wave function.[3] This effect is robustly reproduced by all wave-function-based methods.

TDDFT fails to recover these effects. With all five functionals, TDDFT predicts a positive Δ_{ST} of about 0.20 eV; see Table 2. TDDFT therefore cannot be recommended as a computational method for large-scale screening studies for OLED materials.[37] Interestingly, the correct (negative) Δ_{ST} of Hz can be obtained by calculating the S_1 and T_1 excitation energies with unrestricted Kohn−Sham DFT, taking advantage of the fact that the $^1A_2'$ and $^3A_2'$ states are the lowest states of their respective symmetries. With the B3LYP, PBE0, M06-2X, CAM-B3LYP, and ωB97X-D functionals, Δ_{ST} is obtained as −0.165, −0.232, −0.218, −0.391, and −0.347 eV, respectively, in qualitative agreement with the wave-function-based methods. Analyzing the orbital energies of the unrestricted DFT (UDFT) calculations, a systematic red shift of about 0.2 eV of the energies of the singly occupied HOMO and LUMO of the UDFT calculation for the singlet state compared to the UDFT calculation for the triplet state is observed for the B3LYP, PBE0, and M06-2X functionals, which lowers the energy of the singlet excited state relative to the triplet excited state. For the range-separated functionals, which slightly overestimate the inverted singlet−triplet gap, the effect is more pronounced, with the orbital energies of the singlet calculations being lower by 0.3−0.4 eV than the orbital energies of the triplet calculations. The qualitative effect of spin polarization is thus clearly visibly in the unrestricted DFT orbital picture.

The equilibrium geometries of the S_1 and T_1 excited states of Hz were optimized with the ADC(2) method. The adiabatic (minimum-to-minimum) excitation energies of the S_1 and T_1 states are 2.488 and 2.777 eV, respectively. The vibrational stabilization energy therefore is 0.081 eV in the S_1 state and 0.074 eV in the T_1 state. These unusually small vibrational stabilization energies reflect the rigidity of the fused ring structure of Hz. The exceptionally weak electron-vibration coupling in the S_1 and T_1 states is favorable for solar energy harvesting with the Hz chromophore, as will be discussed below.

To explore the S_1 and T_1 PE surfaces in the vicinity of the FC region, we computed linearly interpolated scans between the ground-state equilibrium geometry and the S_1 and T_1 equilibrium geometries. The energy profiles of the S_1 and T_1 states along these scans are shown in Figure 2. The S_1 and T_1 energy profiles are essentially parallel without indications of crossings of the PE surfaces. Notably, the energy minimum of the T_1 state (2.777 eV) is higher in energy than the vertical excitation energy of the S_1 state (2.569 eV). The very small changes of the S_0 energy along these scans reflect the fact that

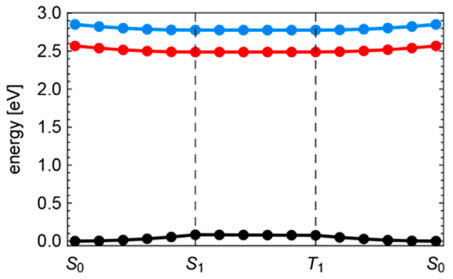

Figure 2. Energy profiles of linearly interpolated scans between the S_0 minimum geometry, the S_1 minimum geometry, and the T_1 minimum geometry of Hz. The energy of the T_1 state (blue) is above the energy of the S_1 state (red) throughout. Black, S_0 state.

the equilibrium geometries of the S_0, S_1, and T_1 states are very similar. These findings tentatively indicate that the rate of ISC from the T_1 state to the S_1 state of Hz is comparatively small.

To support the assignment of spectroscopic characterizations of the long-lived S_1 and T_1 states of Hz (see below), we computed the $S_1 \rightarrow S_n$ and $T_1 \rightarrow T_n$ excitation energies and oscillator strengths with the ADC(2) method. Figure 3A

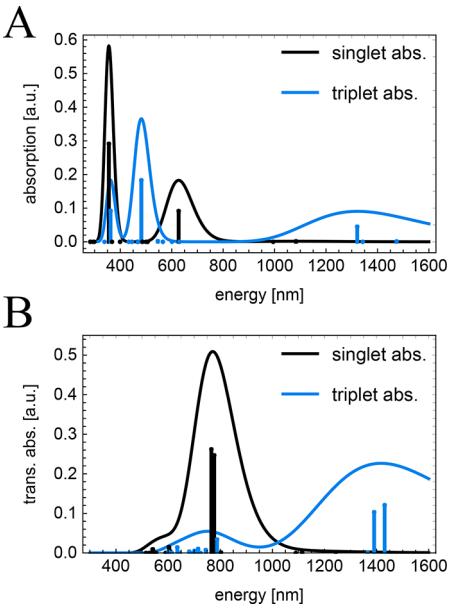

Figure 3. Excited-state absorption spectra of (A) Hz and (B) TAHz in the singlet manifold (black) and triplet manifold (blue). The lines are convoluted with a Gaussian function with a width of 0.3 eV.

displays simulated excited-state absorption spectra of Hz. The line positions represent the excitation energies, and the heights of the lines represent the oscillator strengths. The excited-state absorption spectrum in the singlet manifold (black) exhibits two dipole-allowed transitions, at 1.98 (627 nm) and 3.49 eV (356 nm). The triplet absorption spectrum (blue) exhibits three dipole-allowed transitions at 0.94 (1322 nm), 2.57 (483 nm), and 3.42 eV (363 nm). All these transitions occur among $\pi\pi^*$ excited states of Hz. Figure 3 shows that the long-lived S_1 and T_1 excited states can potentially be identified by their absorption spectra. The lowest absorption band of the T_1 state (0.94 eV, 1322 nm) is substantially lower in energy than the lowest absorption band of the S_1 state (1.98 eV, 627 nm).

3.2. Heptazine Derivatives. We computed the vertical excitation energies of three derivatives of Hz—trichlorohepta-

DOI: 10.1021/acs.jpca.9b06215
J. Phys. Chem. A 2019, 123, 8099−8108

zine (TClHz), tricyanoheptazine (TCNHz), and TAHz—with the ADC(2) method. The S_1 and T_1 vertical excitation energies of these three Hz derivatives are listed in Table 3 together with

Table 3. Lowest Singlet (S_1) and Triplet (T_1) Vertical Excitation Energies and Singlet−Triplet Energy Gap Δ_{ST} of Different Heptazine Derivatives, Calculated at the ADC(2) Level[a]

molecule	S_1	T_1	Δ_{ST}
Hz	2.569	2.851	−0.282
TAHz	2.623	2.872	−0.249
TClHz	2.767	3.062	−0.295
TCNHz	2.282	2.520	−0.238

[a]Geometries were optimized at the MP2 level.

the excitation energies of Hz. For all three derivatives, the HOMO and the LUMO are exclusively localized on the Hz frame; see Figure S1 in the Supporting Information. The S_1 and T_1 states are nearly pure HOMO−LUMO transitions in all three derivatives. Correspondingly, the S_1 and T_1 excitation energies of the three derivatives are close to those of Hz.

In TAHz and TClHz, the substituents are weakly electron-donating, which leads to a slight increase of the S_1 and T_1 excitation energies. The cyano groups in TCNHz, on the other hand, are electron-withdrawing, which results in a moderate lowering of the S_1 and T_1 energies by about 0.3 eV. It is seen that Δ_{ST} is robustly negative, varying between −0.238 and −0.295 eV. It can be concluded that the S_1/T_1 inversion is an intrinsic and robust property of the heptazine chromophore and is negligibly affected by electron-donating and electron-withdrawing substituents.

The excited-state absorption spectra of TAHz are overall similar to those of Hz (cf. Figure 3B). The lowest absorption bands in the triplet manifold are at 0.88 (1410 nm) and 1.65 eV (752 nm). The lowest absorption band in the singlet manifold also is at 1.65 eV (752 nm) and has a significantly higher oscillator strength than the triplet band.

One could initially regard the unusually long decay time of the TAHz emission, with τ on the order of 300 ns,[34] as indicating that a long-lived triplet state contributes to the PL lifetime in some manner, for example, by phosphorescence or reverse intersystem crossing and thermally activated delayed fluorescence (TADF). Indeed, depending on the measurement conditions, the phosphorescence lifetime of the ubiquitous triplet material, ruthenium(II) tris-bipyridine $[Ru(bpy)_3]^{2+}$, has been well documented to be on the order of 500−900 ns.[38] We measured the time-dependent PL decay of TAHz in toluene on the microsecond time scale to investigate whether the presence of molecular oxygen, a known triplet quencher, has any influence on the TAHz excited state decay dynamics. The resulting luminescence lifetime data shown in Figure 4A demonstrate that we observe only monoexponential decay over two decades in intensity, with no discernible influence on the

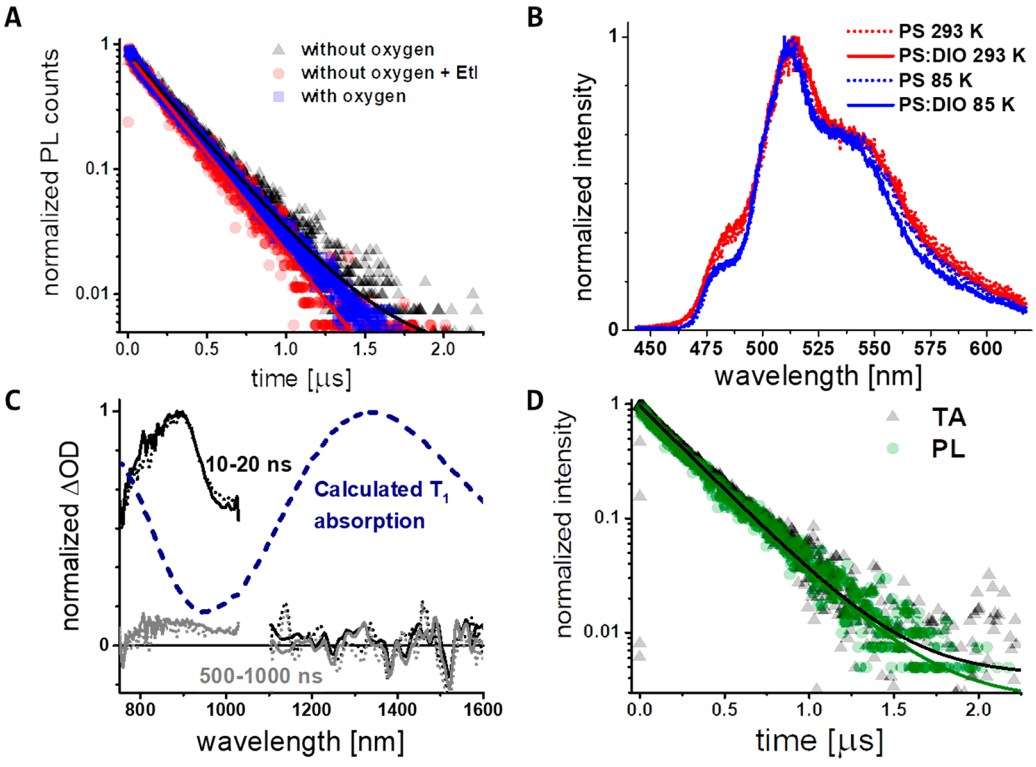

Figure 4. (A) Emission lifetimes of TAHz in toluene show very little dependence on the presence of oxygen or a heavy atom. Comparing emissions with (blue) and without oxygen (black), we do not see any evidence of thermally activated delayed florescence. (B) The emission spectra of TAHz in toluene with (solid) and without (dotted) a heavy atom present in a polystyrene matrix at 298 (red) and 80 K (blue) do not show evidence of phosphorescence. (C) Transient absorption data with (dotted) and without (solid) a heavy atom present at early (black) and long (gray) time scales show no significant difference. Notably, we see no long-lived signal in the NIR region where a strong triplet absorption transition is predicted by the calculations (dashed line). (D) Decay kinetics of the photoluminescence (green circles) matches the decay of the prominent spectral feature at 900 nm seen in transient absorption measurements (black triangles), suggesting that we only see the S_1 absorption feature in our TA measurements.

DOI: 10.1021/acs.jpca.9b06215
J. Phys. Chem. A 2019, 123, 8099−8108

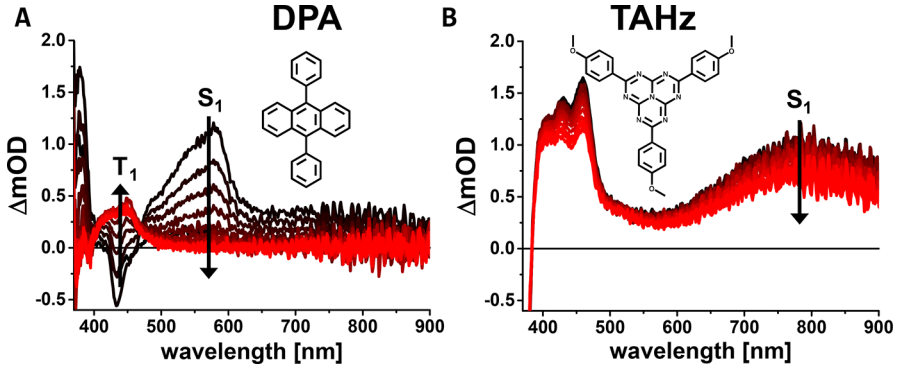

Figure 5. Transient absorption spectral traces from 2 to 100 ns (black to red) for chromophores DPA (A) and TAHz (B) in 1:1 toluene:Br-octane solutions. We observe a clear isosbestic behavior in the case for DPA: the singlet absorption at 550 nm is converted to the lower-lying triplet with a characteristic absorption at 450 nm. However, in the case of TAHz, we only see the decrease across the spectral region. The TAHz PL decay matches the decay of the large feature at 800 nm. This suggests that there is no lower-lying triplet for the heavy-atom-enhanced intersystem crossing to be formed from the long-lived singlet excited state.

lifetime from molecular oxygen and no perceptible biphasic character that would imply a contribution from a delayed fluorescence component. The fact that we observe negligible dependence of the emission lifetime on the presence of molecular oxygen, which would quantitatively quench any molecular triplet state T_1 with an energy of >1.0 eV on this time scale, renders the possibility unlikely that TADF plays any role in extending the PL decay time in TAHz. Interestingly, as Figure 4A also demonstrates, the emission lifetime is virtually independent of the presence of external heavy atom sources, such as ethyl iodide (EtI), that are commonly used to sensitize intersystem crossing to populate the T_1 state. The PL quantum yield (PLQY) also exhibits no dependence on the presence of EtI. The fact that introducing an external heavy atom to enhance the intersystem crossing rate constant does not quench the singlet PLQY or lifetime is consistent with the absence of a lower-lying triplet state that would otherwise act as a nonradiative energy sink.

The kinetics data in Figure 4A do not provide any spectral information that could report on the possible role of phosphorescence from the T_1 state. To discern whether phosphorescence contributes to the overall TAHz PL signal, we present in Figure 4B time-averaged low-temperature PL spectra for TAHz with and without diiodooctane (DIO) as an external heavy atom source. We have previously employed this method in our laboratory to detect extremely weak phosphorescence signatures from organic chromophores that do not exhibit measurable steady-state triplet emission in the absence of an external heavy atom.[35] Nevertheless, in the case of TAHz, the PL spectra that we collect with and without the presence of an external heavy atom are virtually indistinguishable. We observe no evidence for phosphorescence from TAHz, even affixed in an inert polystyrene matrix at low temperatures in the presence of a heavy atom. Therefore, the lack of quenching with EtI in Figure 4A cannot be explained by increased phosphorescence.

While our PL measurements indicate that the emission properties of TAHz do not involve a low-lying triplet state, the strong fluorescence signal may mask any contribution from a triplet-associated emission component. Therefore, in order to more clearly reveal how the predicted S_1/T_1 energy inversion manifests in the excited-state dynamics of TAHz, we turned to microsecond transient absorption (TA) measurements. Figure 4C shows TA spectra of TAHz in toluene with and without oxygen present at both early and late times. In particular, looking in the region of the theoretically predicted T_1 absorption (~1300 nm, see Figure 3B), we do not see any measurable induced absorption signal for either sample in Figure 4C, while the S_1 absorption near 900 nm is clearly observed. Moreover, Figure 4D shows that the decay of the TA signal overlays with the fluorescence decay. The essentially identical kinetic data for the TA feature and the fluorescence suggest that this feature is attributable solely to the singlet excited state absorption.

As a means of benchmarking the peculiar photophysical behavior that TAHz exhibits as a result of its inverted S_1/T_1 energy landscape, we compare the excited-state dynamics of TAHz against an archetypal organic fluorophore in the presence of an external heavy atom. We chose diphenyl anthracene (DPA) as a model organic fluorophore due to its well-documented near-unity PLQY, implying that very few triplets are readily formed in DPA under illumination. In the presence of bromooctane, the evolution of the DPA TA signal in Figure 5A is markedly different from the spectral evolution that TAHz exhibits in Figure 5B. Figure 5A shows the transient absorption traces of DPA in a toluene:bromooctane solution ranging from 2 to 100 ns. We observe a clear isosbestic point near 465 nm as the DPA S_1 state relaxes by ISC to the lower-energy T_1 state. The DPA S_1 induced absorption signature at 560 nm dominates the DPA TA spectrum at 2 ns in black, but undergoes complete decay by 100 ns, as shown in the red trace. The concomitant rise of the T_1-T_n absorption signal at 450 nm results from the DPA singlets being converted into DPA triplets. Conversely, in Figure 5B, TAHz exhibits no clear signs of interconversion among excited states. Instead, we observe only a decrease in the signal amplitude over this spectral range. We do not observe growth of a new state which would accompany conversion to the triplet manifold. The decay kinetics at 450 and 800 nm overlap with the PL decay, suggesting that these features are attributable to the TAHz S_1 absorption. We do not see any long-lived signal intensity near 800 or 1400 nm (see Figure S5), as predicted by theory, which would also suggest that we do not see long-lived triplet formation.

3.3. Heptazine Oligomers. The polymer melon, first prepared by Berzelius and Justus von Liebig and widely referred to as graphitic carbon nitride (g-CN) in the literature,[15−17] is assumed to consist of one-dimensional or

DOI: 10.1021/acs.jpca.9b06215
J. Phys. Chem. A 2019, 123, 8099−8108

two-dimensional oligomers of Hz units which are connected by imine (NH) groups.[39−42] The NH linkages are formed by the condensation of melem (triaminoheptazine) units which tend to form linear chains.[40,41]

To investigate the effect of oligomerization on S_1/T_1 inversion, we computed the S_1 and T_1 vertical excitation energies for linearly connected oligomers of melem with the ADC(2) method. The structures of the oligomers are shown in Figure 6. The S_1 and T_1 excitation energies and the singlet−

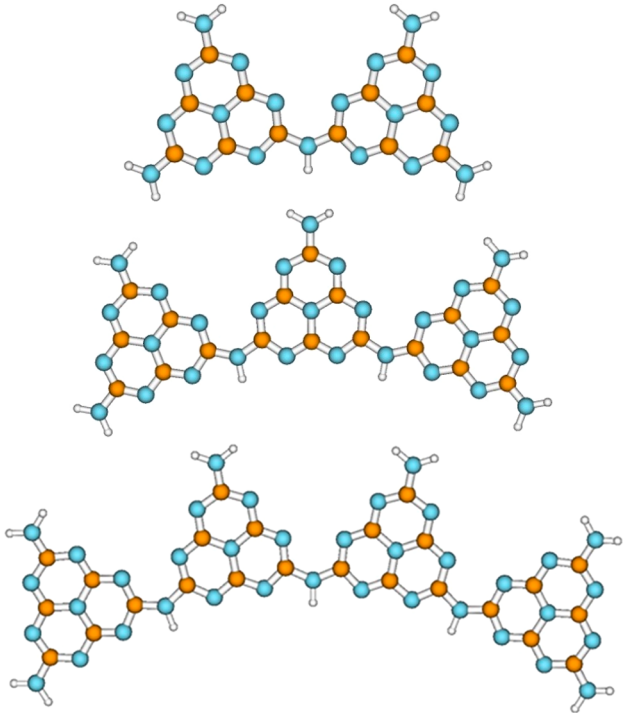

Figure 6. Molecular structures of the melem oligomers considered in this work.

Table 4. Lowest Singlet (S_1) and Triplet (T_1) Vertical Excitation Energies and Singlet−Triplet Energy Gap Δ_{ST} (in eV) of Melem (Triaminoheptazine) Oligomers, Calculated with the ADC(2) Method[a]

oligomer	S_1	T_1	Δ_{ST}
melem dimer	3.480	3.685	−0.205
melem trimer	3.284	3.536	−0.252
melem tetramer	3.265	3.510	−0.245

[a]Geometries were optimized at the MP2 level.

triplet gap Δ_{ST} are given in Table 4 for the dimer, trimer, and tetramer. The S_1 and T_1 excitation energies of melem and its oligomers are higher than those of Hz due to the strong electron-donating character of the amino groups. Δ_{ST}, on the other hand, is found to be negative and close to the value of −0.28 eV obtained for the Hz monomer. It turns out to be independent of the chain length. It can be concluded that oligomerization has negligible impact on Δ_{ST}. The S_1/T_1 inversion is an intrinsic property of the Hz chromophore which is not affected by slight distortions of the Hz monomers in oligomers and is preserved in polymeric carbon nitrides.

Finally, we investigated whether stacking interactions between Hz momomers could affect Δ_{ST}. The ground-state geometry of the stacked Hz dimer is displayed in Figure 7. The

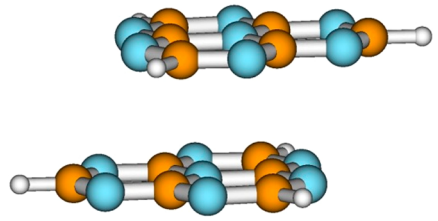

Figure 7. Equilibrium geometry of the lowest-energy conformer of the stacked Hz dimer, optimized at the MP2 level.

dimer exhibits two narrowly spaced S_1, S_2 states and the corresponding triplet states, T_1, T_2 (Table 5). The gaps Δ_{ST} of

Table 5. Lowest Singlet (S_1, S_2) and Triplet (T_1, T_2) Vertical Excitation Energies (in eV) of the Stacked Hz Dimer, Calculated with the ADC(2) Method[a]

state	energy
S_1	2.498
S_2	2.510
T_1	2.777
T_2	2.781

[a]The geometry of the dimer was optimized at the MP2 level.

the two singlet−triplet pairs are −0.27 and −0.28 eV, respectively, essentially identical with the Hz monomer. It is therefore unlikely that stacking interactions in polymeric g-C_3N_4 have a significant effect on the intrinsic singlet−triplet gap of this material, although the bands emerging from the S_1 and T_1 states of the monomer may possibly overlap in the polymer.

4. DISCUSSION

The inversion of the S_1 and T_1 states in Hz and Hz derivatives is a finding which has potentially far-reaching consequences for organic optoelectronics. According to spin statistics, the recombination of charge carriers (electrons and holes) in optoelectronic materials produces singlet and triplet excitons in the ratio 1:3. Because the triplet excitons do not contribute to fluorescence, the fluorescence quantum yield cannot exceed 25%. Adachi and co-workers invoked the concept of reverse intersystem crossing from triplet excitons to generate thermally activated delayed fluorescence (TADF) as a means of boosting the fluorescence quantum yield beyond the commonly regarded statistical limit of 25%.[10,11] The crucial requirement for TADF is a small (positive) Δ_{ST} in combination with a reasonable radiative decay rate ($k_{rad} > 10^6$ s^{-1}). Thermally enhanced reverse ISC from the T_1 state to the S_1 state can then lead, in principle, to a fluorescence quantum yield near 100%. Small Δ_{ST} of the order of 100 meV can be achieved in supramolecular systems consisting of spatially well-separated electron donor and electron acceptor units.[10] Numerous materials tailored for TADF were synthesized and tested for their light-emitting efficiencies.[12,13] The existence of inverted S_1 and T_1 states in Hz-derived materials offers an alternative possibility to harvest triplet excitations. In materials with a negative Δ_{ST}, reverse ISC from the T_1 to the S_1 state is expected to be efficient, as it is exothermic. The back reaction

DOI: 10.1021/acs.jpca.9b06215
J. Phys. Chem. A 2019, 123, 8099−8108

(ISC from S_1 to T_1) is unlikely, as it is endothermic. In this scenario, prompt fluorescence and delayed fluorescence are expected as in TADF, but with an opposite temperature dependence. At low temperatures, no thermal energy is available for the endothermic back reaction (ISC from S_1 to T_1), which should result in a fluorescence yield which increases at lower temperatures.

In 2013, Adachi and co-workers reported on a highly efficient OLED using Hz as electron acceptor and a butyl-substituted phenylaniline (TDA) as electron donor.[43] With this OLED, exceptional fluorescence efficiencies of 95% in toluene and 91% in a solid film were achieved, which is one of the best performances reported for OLEDs.[43] While the spectra of the prompt photoluminescence and the delayed photoluminescence are identical, it is unusual that the intensity of the delayed component was found to decrease with increasing temperature, which is the opposite behavior as expected and observed in other TADF systems.[43] A possible explanation of this phenomenon could be inverted S_1 and T_1 states in Hz; that is, ISC occurs exothermically from T_1 to S_1 rather than by thermally induced reverse ISC.

A different piece of evidence hinting at inverted S_1/T_1 states of the Hz chromophore has been reported for Hz-based polymeric carbon nitride materials. N-heterocycles generally exhibit low-lying triplet excited states which readily generate singlet oxygen ($^1O_2$) from triplet oxygen. However, an ultralow yield of $^1O_2$ has unexpectedly been observed for irradiated g-CN materials.[44−46] This observation is a strong indication that the lowest excited state with the longest lifetime in g-CN materials is a singlet state rather than a triplet state.

The most widespread application of carbon nitride materials, by far, is photocatalytic hydrogen evolution from water.[16,17] In hundreds of articles published in the past five years it is stated that g-CN is a relatively poor photocatalytic material for hydrogen evolution from water because charge carriers (electrons and holes) generated by exciton dissociation tend to recombine at defects of the polymer, leading to photoluminescence, which is detrimental. In this scenario, formation of long-lived excitons is a loss mechanism which should be prevented or at least minimized. An alternative scenario has been proposed, in which the Hz chromophore directly oxidizes hydrogen-bonded water molecules by an excited-state proton-coupled electron-transfer (PCET) reaction.[47,48] In this alternative scenario, one rather would like to maximize the excited-state lifetime to foster the endothermic oxidation of water molecules. While long excited-state lifetimes have historically been achieved by promoting intersystem crossing to the triplet manifold, this process comes with several drawbacks.[49] For one, the energy gap between singlet and triplet excited states can be quite large, sometimes over 1 eV downhill, reducing the energy available to drive the desired photochemistry. Additionally, triplet excitons can be readily quenched by molecular oxygen (which is a triplet in its ground state), forming highly reactive singlet oxygen that can drive chromophore decomposition. On the other hand, if a singlet exciton is the lowest energy excited state of the chromophore, the light absorber could be more stable in the presence of oxygen and thus broaden the application space to include photochemical reactions under atmospheric conditions, such as CO_2 conversion. Recently, it has been shown that TAHz exhibits a long singlet lifetime ($\tau_f \sim 300$ ns) in toluene, undergoes PCET with water, and is stable in the presence of oxygen.[34]

Several features of the Hz chromophore emerge from the recent joint computational, spectroscopic, and kinetic investigations which together predestine this chromophore for photocatalytic water oxidation. (i) The rigidity of the fused ring structure of Hz suppresses internal conversion (IC) from the S_1 state to the S_0 state. (ii) The S_1/T_1 inversion eliminates ISC as a quenching channel in Hz. (iii) The S_1-S_0 radiative transition is symmetry-forbidden and additionally suppressed by nonoverlapping HOMO and LUMO orbitals. (iv) The specific structures of HOMO and LUMO render the peripheral nitrogen atoms of Hz extremely electron deficient in the $S_1(\pi\pi^*)$ excited state, which provides the driving force for the abstraction of electrons from hydrogen-bonded water molecules.[47] The first three properties of the Hz chromophore lead to an exceptionally long intrinsic S_1 lifetime of hundreds of nanoseconds during which the energy of the absorbed photon can be stored as chemical energy and can be used for the oxidation of water.

5. CONCLUSIONS

Ab initio electronic-structure calculations predict that the S_1 state is located below the T_1 state in the Hz chromophore. This exceptional property, as well as the small radiative rate and the very low IC rate to the electronic ground state, lead to an exceptionally long lifetime of the photon energy stored in the S_1 state of Hz. The calculations provide evidence that the negative Δ_{ST} is a robust property of the Hz chromophore. Neither chemical substitution nor oligomerization appears to impact the inverted S_1/T_1 energy gap. The observed luminescence lifetimes and the lack of a heavy atom effect and sensitivity to oxygen confirm the fluorescence character of the luminescence of TAHz. The nanosecond time scales of molecular diffusion place an inherent requirement on the necessary excited-state lifetime that must be sustained in order to achieve productive photon-driven chemical transformations. For this reason, access to triplet excited states with long lifetimes on the order of hundreds of nanoseconds has long made heavy metal complexes a favored class of photoactive materials among researchers investigating photoredox catalysis and solar fuel generation. It is remarkable that heptazine chromophores can offer a comparable range of excited-state lifetimes in their singlet manifolds. The energy losses inherent in intersystem crossing transitions can thereby be avoided.

Once dubbed "the mystery molecule",[40,50] Hz no longer is a mystery thanks to modern electronic-structure theory. Hz rather emerges as a chromophore with truly unique properties which can be exploited in organic optoelectronics, photocatalytic water oxidation, and carbon dioxide recycling to renewable fuels.

■ ASSOCIATED CONTENT

Supporting Information

The Supporting Information is available free of charge on the ACS Publications website at DOI: 10.1021/acs.jpca.9b06215.

HOMOs and LUMOs of three Hz derivatives; additional experimental data showing kinetics of low temperature TR-PL and additional spectral comparisons; kinetic comparisons of PL and TA decays for both DPA and TAHz confirming singlet assignments in TA (PDF)

DOI: 10.1021/acs.jpca.9b06215
J. Phys. Chem. A 2019, 123, 8099−8108

AUTHOR INFORMATION

Corresponding Author

*E-mail: domcke@ch.tum.de.

ORCID

Emily J. Rabe: 0000-0002-9397-049X
Cody W. Schlenker: 0000-0003-3103-402X
Andrzej L. Sobolewski: 0000-0001-5718-489X
Wolfgang Domcke: 0000-0001-6523-1246

Notes

The authors declare no competing financial interest.

ACKNOWLEDGMENTS

This work has been supported by the Munich Centre for Advanced Photonics (MAP). J.E. acknowledges support by the International Max Planck Research School of Advanced Photon Science (IMPRS-APS). A.L.S. acknowledges support by the Alexander von Humboldt Research Award. C.W.S. acknowledges that a portion of this material is based upon work supported by the U.S. National Science Foundation (NSF) under Grant No. CHE-1846480. S.R.P. acknowledges this material is based upon work supported by the National Science Foundation Graduate Research Fellowship Program under Grant No. DGE-1762114. Any opinions, findings, and conclusions or recommendations expressed in this material are those of the author(s) and do not necessarily reflect the views of the National Science Foundation.

REFERENCES

(1) Hund, F. *Linienspektren und Periodisches System der Elemente*; Springer: Berlin, 1927.
(2) Birks, J. B. *Photophysics of Aromatic Molecules*; Wiley: New York, 1970.
(3) Koseki, S.; Nakajima, T.; Toyota, A. Violation of Hund's Multiplicity Rule in the Electronically Excited States of Conjugated Hydrocarbons. *Can. J. Chem.* **1985**, *63*, 1572−1579.
(4) Segal, M.; Singh, M.; Rivoire, K.; Difley, S.; Van Voorhis, T.; Baldo, M. A. Extrafluorescent Electroluminescence in Organic Light-Emitting Diodes. *Nat. Mater.* **2007**, *6*, 374−378.
(5) Difley, S.; Beljonne, D.; Van Voorhis, T. On the Singlet-Triplet Splitting of Geminate Electron-Hole Pairs in Organic Semiconductors. *J. Am. Chem. Soc.* **2008**, *130*, 3420−3427.
(6) Zhang, C.-R.; Sears, J. S.; Yang, B.; Aziz, S. G.; Coropceanu, V.; Bredas, J.-L. Theoretical Study of the Local and Charge-Transfer Excitations in Model Complexes of Pentacene-C60 Using Tuned Range-Separated Hybrid Funtionals. *J. Chem. Theory Comput.* **2014**, *10*, 2379−2388.
(7) Bittner, E. R.; Lankevich, V.; Gelinas, S.; Rao, A.; Ginger, D. A.; Friend, R. H. How Disorder Controls the Kinetics of Triplet Charge Recombination in Semiconducting Organic Polymer Photovoltaics. *Phys. Chem. Chem. Phys.* **2014**, *16*, 20321−20328.
(8) De Kanter, F. J. J.; Kaptein, R. CIDNP and Triplet-State Reactivity of Biradicals. *J. Am. Chem. Soc.* **1982**, *104*, 4759−4766.
(9) Doubleday, J. C.; Turro, N. C.; Wang, J.-F. Dynamics of Flexible Triplet Biradicals. *Acc. Chem. Res.* **1989**, *22*, 199−205.
(10) Uoyama, H.; Goushi, K.; Shizu, K.; Nomura, H.; Adachi, C. Highly Efficient Organic Light-Emitting Diodes from Delayed Fluorescence. *Nature* **2012**, *492*, 234−238.
(11) Goushi, K.; Yoshida, K.; Sato, K.; Adachi, C. Organic Light-Emitting Diodes Employing Efficient Reverse Intersystem Crossing for Triplet-to-Singlet State Conversion. *Nat. Photonics* **2012**, *6*, 253−258.
(12) Tao, Y.; Yuan, K.; Chen, T.; Xu, P.; Li, H.; Chen, R.; Zheng, C.; Zhang, L.; Huang, W. Thermally Activated Delayed Fluorescence Materials Towards the Breakthrough of Organoelectronics. *Adv. Mater.* **2014**, *26*, 7931−7958.
(13) Jou, J.-H.; Kumar, S.; Agrawal, A.; Li, T.-H.; Sahoo, S. Approaches for Fabricating High Efficiency Organic Light Emitting Diodes. *J. Mater. Chem. C* **2015**, *3*, 2974−3002.
(14) Kollmar, H.; Staemmler, V. Violation of Hund's Rule by Spin Polarization in Molecules. *Theoret. Chim. Acta (Berl.)* **1978**, *48*, 223−239.
(15) Wang, X.; Maeda, K.; Thomas, A.; Takanabe, K.; Xin, G.; Carlsson, J. M.; Domen, K.; Antonietti, M. A Metal-Free Polymeric Photocatalyst for Hydrogen Production from Water Under Visible Light. *Nat. Mater.* **2009**, *8*, 76−80.
(16) Ong, W.-J.; Tan, L.-L.; Ng, Y. H.; Yong, S.-T.; Chai, S.-P. Graphitic Carbon Nitride (g-C3N4)-Based Photocatalysts for Artificial Photosynthesis and Environmental Remediation: Are we a Step Closer to Achieving Sustainability? *Chem. Rev.* **2016**, *116*, 7159−7329.
(17) Wen, J.; Xie, J.; Chen, X.; Li, X. A Review on g-C3N4-Based Photocatalysts. *Appl. Surf. Sci.* **2017**, *391*, 72−123.
(18) Schirmer, J. Beyond the Random-Phase Approximation: A New Approximation Scheme for the Polarization Propagator. *Phys. Rev. A: At., Mol., Opt. Phys.* **1982**, *26*, 2395−2416.
(19) Christiansen, O.; Koch, H.; Jorgensen, P. The Second-Order Approximate Coupled Cluster Singles and Doubles Model CC2. *Chem. Phys. Lett.* **1995**, *243*, 409−418.
(20) Stanton, J. F.; Bartlett, R. J. The Equation of Motion Coupled-Cluster Method. A Systematic Biorthogonal Approach to Molecular Excitation Energies, Transition Probabilities, and Excited State Properties. *J. Chem. Phys.* **1993**, *98*, 7029−7039.
(21) Roos, B. O. The Complete Active Space Self-Consistent Field Method and its Applications in Electronic-Structure Calculations. *Adv. Chem. Phys.* **2007**, *69*, 399−445.
(22) Andersson, K.; Malmqvist, P. A.; Roos, B. O. Second-Order Perturbation Theory with a Complete Active Space Self-Consistent Field Reference Function. *J. Chem. Phys.* **1992**, *96*, 1218−1226.
(23) Becke, A. D. Density-Functional Thermochemistry. III. The Role of Exact Exchange. *J. Chem. Phys.* **1993**, *98*, 5648−5652.
(24) Lee, C.; Yang, W.; Parr, R. G. Development of the Colle-Salvetti Correlation-Energy Formula into a Functional of the Electron Density. *Phys. Rev. B: Condens. Matter Mater. Phys.* **1988**, *37*, 785−789.
(25) Perdew, J. P.; Ernzerhof, M.; Burke, K. Rationale for Mixing Exact Exchange with Density Functional Approximations. *J. Chem. Phys.* **1996**, *105*, 9982−9985.
(26) Zhao, Y.; Truhlar, D. G. The M06 Suite of Density Functionals for Main Group Thermochemistry, Thermochemical Kinetics, Noncovalent Interactions, Excited States, and Transition Elements: Two New Functionals and Systematic Testing of Four M06-Class Functionals and 12 Other Functionals. *Theor. Chem. Acc.* **2008**, *120*, 215−241.
(27) Yanai, T.; Tew, D. P.; Handy, N. C. A New Hybrid Exchange−Correlation Functional Using the Coulomb-Attenuating Method (CAM-B3LYP). *Chem. Phys. Lett.* **2004**, *393*, 51−57.
(28) Chai, J.-D.; Head-Gordon, M. Systematic Optimization of Long-Range Corrected Hybrid Density Functionals. *J. Chem. Phys.* **2008**, *128*, 084106.
(29) Dunning, T. H., Jr. Gaussian Basis Sets for Use in Correlated Molecular Calculations. I. The Atoms Boron Through Neon and Hydrogen. *J. Chem. Phys.* **1989**, *90*, 1007−1023.
(30) *TURBOMOLE*, version 6.3; A Development of University Karlsruhe and Forschungszentrum Karlsruhe GmbH, 1989−2007. Since 2007, TURBOMOLE GmbH: 2011.
(31) Shao, Z.; Gan, Z.; Epifanovsky, E.; Gilbert, A. T.; Wormit, M.; Kussmann, J.; Lange, A. W.; Behn, A.; Deng, J.; Feng, X.; et al. Advances in Molecular Quantum Chemistry Contained in the Q-Chem 4 Program Package. *Mol. Phys.* **2015**, *113*, 184−215.
(32) Werner, H.; Knowles, P.; Knizia, G.; Manby, F.; Schütz, M.; Celani, P.; Györffy, W.; Kats, D.; Korona, T.; Lindh, R. *MOLPRO, 2012.1, A Package of Ab Initio Programs*; 2012. See http://www.molpro.net.

DOI: 10.1021/acs.jpca.9b06215
J. Phys. Chem. A 2019, 123, 8099−8108

(33) Hosmane, R. S.; Rossman, M. A.; Leonard, N. J. Synthesis and Structure of Tri-s-Triazine. *J. Am. Chem. Soc.* **1982**, *104*, 5497−5499.
(34) Rabe, E. J.; Corp, K. L.; Sobolewski, A. L.; Domcke, W.; Schlenker, C. W. Proton-Coupled Electron Transfer from Water to a Model Heptazine-Based Molecular Photocatalyst. *J. Phys. Chem. Lett.* **2018**, *9*, 6257−6261.
(35) Sulas, D. B.; Rabe, E. J.; Schlenker, C. W. Kinetic Competition Between Charge Separation and Triplet Formation in Small-Molecule Photovoltaic Blends. *J. Phys. Chem. C* **2017**, *121*, 26667−26676.
(36) Pershin, A.; Hall, D.; Lemaur, V.; Sancho-Garcia, J.-C.; Muccioli, L.; Zysman-Colman, E.; Beljonne, D.; Olivier, Y. Highly Emissive Excitons with Reduced Exchange Energy in Thermally Activated Delayed Fluorescent Molecules. *Nat. Commun.* **2019**, *10*, 597.
(37) Gomez-Bombarelli, R.; Aguilera-Iparraguirre, J.; Hirzel, T. D.; Duvenaud, D.; Maclaurin, D.; Blood-Forsythe, M. A.; Chae, H. S.; Einzinger, M.; Ha, D.-G.; Wu, T.; et al. Design of Efficient Molecular Organic Light-Emitting Diodes by a High-Throughput Virtual Screening and Experimental Approach. *Nat. Mater.* **2016**, *15*, 1120−1127.
(38) Caspar, J. V.; Meyer, T. J. Photochemistry of Tris(2, 2'-Bipyridine)Ruthenium(2^+) Ion ($Ru(bpy)_3 2^+$). Solvent Effects. *J. Am. Chem. Soc.* **1983**, *105*, 5583−5590.
(39) Wang, Y.; Wang, X.; Antonietti, M. Polymeric Graphitic Carbon Nitride as a Heterogeneous Organocatalyst: from Photochemistry to Multipurpose Catalysis to Sustainable Chemistry. *Angew. Chem., Int. Ed.* **2012**, *51*, 68−89.
(40) Schwarzer, A.; Saplinova, T.; Kroke, E. Tri-s-Triazines (s-Heptazines) - From a ″Mystery Molecule″ to Industrially Relevant Carbon Nitride Materials. *Coord. Chem. Rev.* **2013**, *257*, 2032−2062.
(41) Butchosa, C.; Guiglion, P.; Zwijnenburg, M. A. Carbon Nitride Photocatalysts for Water Splitting: A Computational Perspective. *J. Phys. Chem. C* **2014**, *118*, 24833−24842.
(42) Lau, V. W.; Mesch, M. B.; Duppel, V.; Blum, V.; Senker, J.; Lotsch, B. V. Low-Molecular-Weight Carbon Nitrides for Solar Hydrogen Evolution. *J. Am. Chem. Soc.* **2015**, *137*, 1064−1072.
(43) Li, J.; Nakagawa, T.; MacDonald, J.; Zhang, Q.; Nomura, H.; Miyazaki, H.; Adachi, C. Highly Efficient Organic Light-Emitting Diode Based on a Hidden Thermally Activated Delayed Fluorescence Channel in a Heptazine Derivative. *Adv. Mater.* **2013**, *25*, 3319−3323.
(44) Cui, Y.; Ding, Z.; Liu, P.; Antonietti, M.; Fu, X.; Wang, X. Metal-Free Activation of H_2O_2 by g-C_3N_4 under Visible Light Irradiation for the Degradation of Organic Pollutants. *Phys. Chem. Chem. Phys.* **2012**, *14*, 1455−1462.
(45) Chen, Y.; Zhang, J.; Zhang, M.; Wang, X. Molecular and Textural Engineering of Conjugated Carbon Nitride Catalysts for Selective Oxidation of Alcohols with Visible Light. *Chem. Sci.* **2013**, *4*, 3244−3248.
(46) Wang, H.; Jiang, S.; Chen, S.; Li, D.; Zhang, X.; Shao, W.; Sun, X.; Xie, J.; Zhao, Z.; Zhang, Q.; et al. Enhanced Singlet Oxygen Generation in Oxidized Graphitic Carbon Nitride for Organic Synthesis. *Adv. Mater.* **2016**, *28*, 6940−6945.
(47) Ehrmaier, J.; Karsili, T. N. V.; Sobolewski, A. L.; Domcke, W. Mechanism of Photocatalytic Water Splitting with Graphitic Carbon Nitride: Photochemistry of the Heptazine-Water Complex. *J. Phys. Chem. A* **2017**, *121*, 4754−4764.
(48) Domcke, W.; Ehrmaier, J.; Sobolewski, A. L. Solar Energy Harvesting with Carbon Nitrides and N-Heterocyclic Frameworks: Do We Understand the Mechanism? *ChemPhotoChem.* **2019**, *3*, 10−23.
(49) Sartor, S. M.; McCarthy, B. G.; Pearson, R. M.; Miyake, G. M.; Damrauer, N. H. Exploiting Charge-Transfer States for Maximizing Intersystem Crossing Yields in Organic Photoredox Catalysis. *J. Am. Chem. Soc.* **2018**, *140*, 4778−4781.
(50) Wilson, E. K. A. Prized Collection: Pauling Memorablia. *Chem. Eng. News* **2000**, *78*, 62−63.

DOI: 10.1021/acs.jpca.9b06215
J. Phys. Chem. A 2019, 123, 8099−8108